Definitions and Applications of Dynamic Average Models for Analysis of Power Systems

IEEE Task Force on Dynamic Average Modeling, Working Group on Modeling and Analysis of System Transients Using Digital Programs, Transmission and Distribution Committee, IEEE Power and Energy Society

S. Chiniforoosh, J. Jatskevich, A. Yazdani, V. Sood, V. Dinavahi, J. A. Martinez, and A. Ramirez

***Abstract*—Modeling and analysis of power and power-electronic systems' transients using digital programs enables testing new design concepts in modern electric grid and many industrial and commercial products and applications. This paper gives an overview of dynamic average-value modeling techniques for representing static switching converters for the system-level studies. Concepts and desirable properties of averaged models for conducting large-signal time-domain transient studies and small-signal frequency-domain analysis for control design tasks are discussed. Basic approaches for developing average models for dc/dc and dc/ac converters are briefly reviewed and summarized. Finally, the desirable properties of the average-value models are demonstrated through an example system.**

***Index Terms*—Dynamic average-value modeling, simulation, system transients.**

I. Introduction

MODELING and simulation of power and power-electronic-based systems are essential steps that enable design and verifications of numerous electrical energy systems including modern electric grid and its components, distributed energy resources, as well as electrical systems of ships, aircraft, vehicles, industrial automation, etc. With the development of modern simulation tools, the detailed models of power-electronic components and modules (where the switching of all diodes and transistors is taken into account) may be readily implemented using a number of commercially available digital programs and/or simulators [1]–[12]. It is therefore possible to readily develop models of larger systems from a number of smaller subsystems/modules that can be used for the simulation of systems' transients. However, the use of detailed switching models often leads to significant increase of the required computing time, which in turn often limits the size of the system that can be practically simulated. At the same time, the switching models are also discontinuous and therefore difficult to use for extracting the small-signal characteristics of various modules for the system-level analysis.

The above challenges have led to development of the so-called dynamic average-value models (AVMs) which approximate the original system by "neglecting" or "averaging" the effect of fast switching within a prototypical switching interval. Such dynamic average models have been very successfully used for modeling of distributed DC power systems of spacecraft [13]–[15] and aircraft [16], [17], naval electrical systems [18], [19], and vehicular electric power systems [20]. Average-value modeling has also been often applied to variable speed wind energy systems [21]–[28], where the machines are typically interfaced with the grid using the power electronic converters.

In modern electric power systems, an increasing number of alternative energy sources and storage are being interfaced with the utility grid using power electronic converters. For investigations of future microgrids and distribution automation [29], [30], modeling and development of utility power electronic and FACTS devices [31]–[41], design of control algorithms for the interfacing and coordination of distributed generation [26], [27], [29], [42]–[44], etc., the dynamic average-value models have been used quite intensively and therefore represent an indispensible tool.

This Task Force paper gives an overview of the average-value modeling techniques for representing static switching converters for system-level studies. The paper may be useful to researchers and practicing engineers in the area of electric power and energy systems who are dealing with applications of power electronic components and modules as well as using modern digital simulation tools. The paper reviews the basic concepts and definitions of average-value modeling and gives a summary of different approaches that can be used to develop such models for dc-dc and ac-dc converters. We also demonstrate the desirable properties of such models for large-signal time-domain and small-signal frequency-domain studies.

II. Typical Power Conversion Cells

In modern power and power-electronic-based systems, conversion between ac and dc power as well as changing the

Manuscript received January 18, 2010. First published March 29, 2010; current version published September 22, 2010. Paper no. TPWRD-00038-2010.

Task Force on Dynamic Average Modeling is with the Working Group on Modeling and Analysis of System Transients Using Digital Programs, Transmission and Distribution Committee, IEEE Power and Energy Society.

Task Force Members: S. A. Abdulsalam, U. Annakkage, S. Chiniforoosh, V. Dinavahi, S. Filizadeh, A. Gole, R. Iravani, J. Jatskevich (Chair), H. Karimi, J. Mahseredjian, J. A. Martinez, N. Nair, L. Naredo, T. Noda, J. N. Paquih, J. Peralta, A. Ramirez, A. Rezaei-Zare, M. Rioual, K. Schoder, V. Sood, A. St. Leger, A. Yazdani.

S. Chiniforoosh and J. Jatskevich are with the Department of Electrical and Computer Engineering, University of British Columbia, Vancouver, BC V6T 1Z4, Canada (e-mails: sinach@ece.ubc.ca; jurij@ece.ubc.ca).

Color versions of one or more of the figures in this paper are available online at http://ieeexplore.ieee.org.

Digital Object Identifier 10.1109/TPWRD.2010.2043859

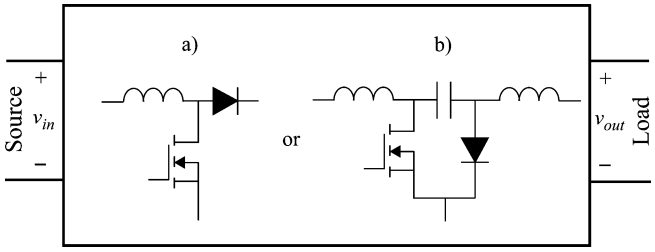

Fig. 1. Basic switched-inductor and switched-capacitor cells.

dc power/voltage levels are done by switching modules, also known as power-processing units or power-electronic building blocks (PEBB) [45]. To better understand the concepts and applications of dynamic average modeling, the typical power conversion topologies are briefly described here. A typical power-processing module is composed of a switching cell and additional passive elements (i.e., inductors, capacitors, resistors) that take part in the energy conversion process and comprise the input/output filters wherever appropriate. In addition to the input and output power ports, switching modules may also have a control input through which the controllable switches, e.g., transistors, thyristors, etc., are turned on and off according to a specific control strategy and/or modulation approach. The switching frequency depends on many factors including the configuration and application of the switching converters, the type of switches, etc., and may vary in a wide range from several times the ac line frequency (50/60 Hz) to hundreds of kHz.

A. Switching Modules

A key element of a basic pulse-width-modulation (PWM) dc-dc converter may be realized using a switched-inductor or switched-capacitor cell shown in Fig. 1(a) and (b), respectively. Opening and closing the controllable switch (transistor) using PWM voltage or current control scheme enables energy conversion from the input source side at one dc voltage level to a different level at the output terminal. As the name implies, the energy in each cell is first stored in the inductor (or the capacitor) and then released to the output side. Typical switching frequency of the transistors may be in the range from tens to hundreds of kHz. To achieve a ripple of voltages and currents within the desirable/acceptable level, appropriate filters are designed at the input and output terminals.

For conversion between dc and ac, a three phase converter may be realized using switching cells depicted in Fig. 2. Depending on whether the upper or the lower switches are conducting, each phase terminal can be connected to either the upper or the lower rail, or left floating if none of the switches are conducting. Hence this topology is often referred to as two-level converter. One of the simplest configurations of Fig. 2(a) is an uncontrollable rectifier that uses the diodes for converting the ac to dc. If the controllable switches in Fig. 2(a) are thyristors or GTOs, then such switching cell can also be used for bi-directional energy conversion. The converter topology of Fig. 2(a) will operate at the switching frequency that is directly determined by the line frequency of the ac side. Such converters are often referred to as line-commutated converters and are particularly useful and cost effective in high voltage/power industrial applications (e.g., HVDC transmission, drives of large industrial motors, etc). The full bridge converter depicted in Fig. 2(b) requires active switches (transistors) that can be switched at a much higher frequency than the ac side line frequency. Various PWM voltage or current control strategies can be used here as well. The energy may be converted from a dc source to supply a load such as an ac motor. Alternatively, the cell can also operate as a rectifier taking the energy from the ac side (which may be an ac generator) and feeding the dc bus to supply other loads. In general, such converter systems may provide bi-directional energy flow during steady state and/or transients and are very common in motor-drives as well as in rectifiers for generator sets. Due to the switching losses, the switching frequency of such converters in power applications may range from several kHz to tens of kHz. However, these converters are often used for medium power level applications and grid interfacing.

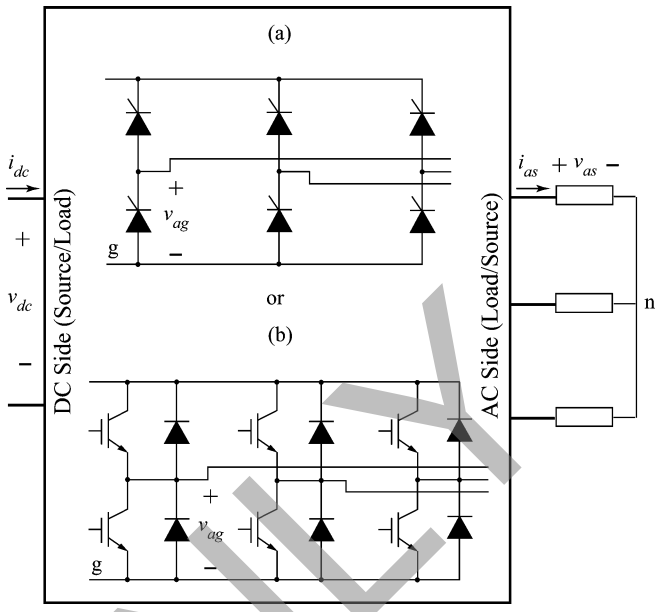

Fig. 2. Typical two-level three-phase converter switching cells. (a) Three-Phase Line-Commutated Converter, (b) Three-Phase Full-Bridge Converter.

To reduce the voltage stress on transistors as well as voltage ripple on the ac side, the basic converter topology of Fig. 2(b) may be extended to provide more than two voltage levels. As an example, a three-level neutral-point clamped (NPC) topology is illustrated in Fig. 3. The main advantages of this converter over the basic two-level topology of Fig. 2(b) include half the off-state voltage across each switch cell and lower harmonic distortion of the ac voltage [38]. In the topology of Fig. 3, an additional voltage level is obtained using the neutral-point of the two capacitors connected in series. Depending on the state of transistors and the direction of the phase current, each phase can be connected to either the lower rail, the neutral-point, or the upper rail; hence the name three-level converter. The operation of this converter can be achieved by coordinated switching of transistors in the two half-bridge converters [46]. The three-level converters with a topology similar to that in Fig. 3 are finding applications in medium-voltage motor drives [47], forced-commu-

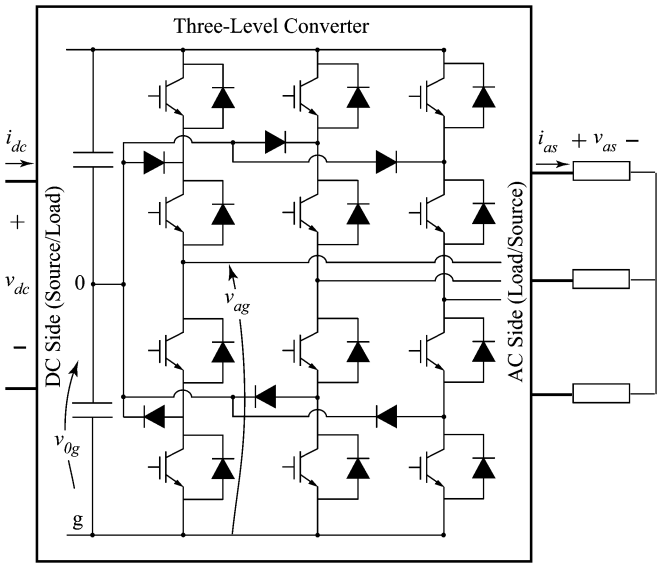

Fig. 3. Typical three-level converter switching cell.

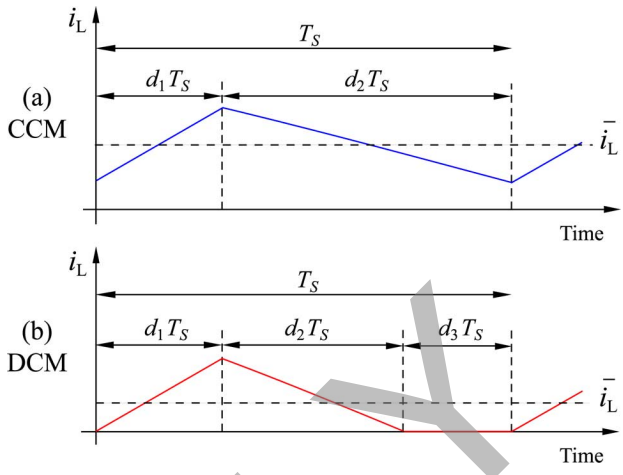

Fig. 4. Typical inductor current waveform of the switched-inductor cell for CCM and DCM operation.

tated HVDC systems [48], and renewable energy systems [49]. As the semiconductor technology matures, such converters may also be considered more favourably for grid interfacing of wind and photovoltaic systems.

B. Operational Modes

The instantaneous on/off conducting states of the active and passive switches (i.e., transistors, thyristors and diodes) determine the topology of each of the switching cells shown in Figs. 1–3. When the converter operates in steady state, a sequence of topologies will become repetitive within each switching interval defining a certain switching pattern. This repetitive pattern of topologies in turn defines the operating mode of a given switching cell. The prototypical switching interval varies for different converters and is the basis for the averaging window when developing average-value models.

For example, the switched-inductor cell of Fig. 1(a) can have three topological states: (i) when the transistor is on and the diode is off; (ii) when the transistor is switched off and the diode is on; and (iii) when both transistor and diode are off. The typical inductor current waveforms for this switching cell are shown in Fig. 4. In continuous conduction mode (CCM), each switching interval T_s is divided into two subintervals d_1T_s and d_2T_s, see Fig. 4(a), corresponding to the topologies (i) and (ii). The variables d_1 and d_2 are the so-called relative duty cycles, which are defined such that $T_s = d_1T_s + d_2T_s$. In discontinuous conduction mode (DCM), the switching pattern also includes the third topological state (iii) in which both switches are off and the current stays at zero for the duration of that subinterval as shown in Fig. 4(b). Hence, the switching interval is divided into three subintervals such that $T_s = d_1T_s + d_2T_s + d_3T_s$.

For the three-phase line commutated converter of Fig. 2(a) the sequence of topological states becomes repetitive for each electrical cycle of the ac line frequency. However, considering the symmetry among the converter phases, a much shorter switching pattern can be selected to define the operational mode. To illustrate this point, the typical phase currents and dc voltage waveforms for the diode rectifier operation are shown in Fig. 5. As can be deduced from Fig. 5, the given operating mode can be characterized by two basic topologies: (i) when only two phases are conducting through 2 diodes; and (ii) when all three phases are conducting current, which requires 3 diodes to conduct as well. This switching pattern of 2–3 conducting diodes repeats. Therefore, based on the currents depicted in Fig. 5, the overall prototypical switching interval T_s is divided into two subintervals: (i) conduction, $t_{\rm cond}$,—when the two phases are conducting full current; and (ii) commutation, $t_{\rm com}$,—when a total of 3 diodes are conducting and the current is being switched (commutated) between two phases, respectively. This conduction-commutation mode is sometimes referred to as 2–3 mode [50]. Other modes for the converter circuit of Fig. 2(a) are also possible depending on the loading conditions and line inductances on the ac and dc sides. For example, with the presence of sufficiently large commutating inductances on the ac side and an inductance on the dc link side, the increasing of load will make the commutation subinterval longer until it extends over the entire switching interval T_s resulting in the new mode 3–3 [50].

In general, an operational mode can be characterized by a sequence of repeated topologies and is a function of loading conditions. Changes in load conditions might lead to a change in the topologies and hence the mode of operation. In more complicated configurations such as 12-pulse or 18-pulse converters, the number and complexity of operational modes significantly increase making it more challenging to develop the average-value models [51], [52]. In many cases, the converter might have been intentionally designed to operate in a certain operational mode in steady-state. However, in order to accurately predict a large-signal transient that could span wide range of operating conditions, the average value model must account for all possible operational modes.

In the three-phase converters of Figs. 2(b) and 3, the switching frequency is typically much higher than that of the line-commutated converter. For a typical power frequency (50/60 Hz) application, the switching frequency may be on the order of several kHz. This allows modulating the voltages

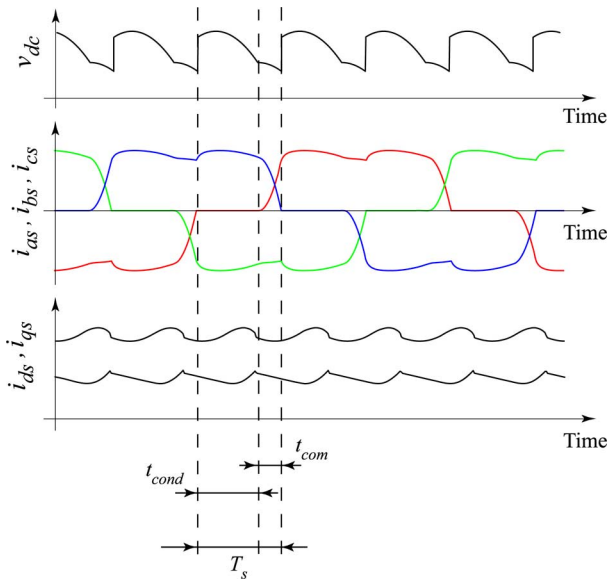

Fig. 5. Typical waveforms of the three-phase line-commutated converter.

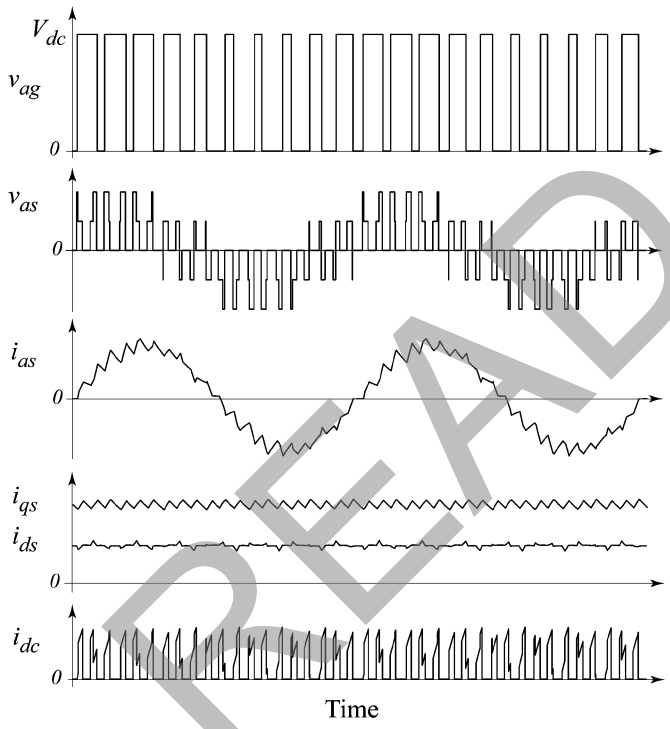

Fig. 6. Typical voltage and current waveforms corresponding to the two-level VSI feeding an inductive load.

and/or currents on the ac side with the desired quality that can approach ideal sinusoidal waveforms. For example, the typical waveforms of the PWM Voltage Source Inverter (VSI) supplying an inductive load are shown in Figs. 6 and 7 for the two- and three-level converters, respectively. As noted in Fig. 6, the phase-to-ground voltage $v_{\rm ag}$ takes only two values (levels), 0 and $V_{\rm dc}$. However, for the three-level converter waveforms depicted in Fig. 7, the phase-to-ground voltage $v_{\rm ag}$ takes three values (levels): $0, V_{0g}$ and $V_{\rm dc}$. This also results in more voltage

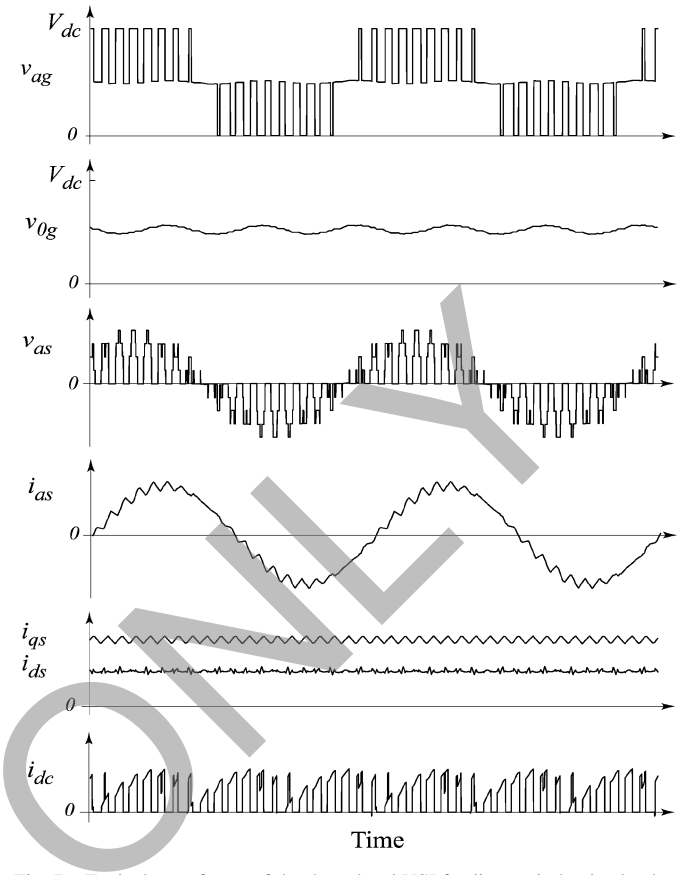

Fig. 7. Typical waveforms of the three-level VSI feeding an inductive load.

levels as seen in the final output phase-to-neutral voltage $v_{\rm as}$ which is seen by the load.

For both converters, it is observed that the phase current (see variable $i_{\rm as}$ in Figs. 6 and 7) essentially consists of the fundamental sinusoidal component with the superimposed high-frequency switching ripples (relatively low content of low-frequency harmonics). The amount of low frequency harmonics in the phase current depends on many factors including the PWM strategy and the switching frequency. Typical modulation strategies include the Sine-Triangle PWM (with 3rd harmonic injection), Space Vector Modulation [46], [56]–[58], etc. The overall prototypical switching interval T_s is determined by the PWM strategy and the switching frequency.

C. Averaging Window

For the purpose of system-level analysis, instead of looking at the instantaneous values of currents and voltages that contain ripple due to switching, it is useful to consider the dynamic average-value that is defined over the length of a switching interval as [53]

$$\bar{f} = \frac{1}{T_s}\int_{t-T_s}^{t} f(t)\mathrm{dt} \tag{1}$$

where $f(t)$ may represent voltage $v(t)$ or current $i(t)$. Observing the averaged inductor current and capacitor voltage in dc-dc converters (see $\overline{i}_L$ in Fig. 4), one can see that these variables will be constant in steady state and otherwise represent slower dynamics of the converter during the transients. The

input and output voltages are often filtered using large electrolytic capacitors that in effect do the averaging. The averaged (or filtered) variables are useful for design of controllers and analysis of dynamic interactions of converter circuits. The idea represented by (1) can be extended [54] such that the resultant averaged model captures also higher-order dynamics, such as those of harmonics; this is referred to as the extended or generalized averaging [55], and is especially instrumental in modeling of resonant converters.

The concept of averaging can also be extended to dc-ac converters. However, simple averaging of the ac variables using (1) over the switching interval will not yield the desired result. Instead, the ac side variables first have to be transformed using an appropriate synchronously rotating qd reference frame [56]. For example, the qd components of the phase current in steady state are also depicted in Figs. 5–7, which shows that the transformed qd variables i_{qs} and $i_{\rm ds}$ are composed of a dc (constant) term and the high-frequency ripple with the same switching interval T_s. Because the qd variables have the dc component that is constant in steady state, these variables can now be used for averaging using (1) in the same way as the variables in the dc-dc converters. The variables on the dc side, e.g., $i_{\rm dc}$, will also contain some ripple due to switching, which often necessitates the use of large capacitors on the dc link, and the averaging concept defined by (1) may be applied here directly.

III. Methods of Constructing Average Models

The objective of Average-Value Modeling (AVM) is to replace the discontinuous switching cells with continuous blocks that represent the averaged behavior of the switching cell within a prototypical switching interval. Obtaining the AVMs generally requires detailed analysis of the switching cells and accurate averaging of the converter waveforms. In this section, some definitions and modeling concepts are described for the dc-dc converters followed by the approaches for dc-ac converters.

A. Circuit/Switch Averaging of DC–DC Converters

Average-value modeling of PWM dc-dc converters can be done by directly averaging the switching cells, e.g., the switched- inductor and capacitor cells depicted in Fig. 1 [57]–[59]. This method is sometimes also referred to as averaged-switch modeling and leads to a unified model for a class of switching cells.

Using circuit averaging, the active/passive switch pair in the switched-inductor cell of Fig. 8(a) is replaced with dependent sources which are functions of the control duty cycle d_1 and the averaged values of the cell's terminal variables. The corresponding equivalent cell is shown in Fig. 8(b). Such models can be readily obtained analytically for continuous conduction mode (CCM) if parasitics are neglected [58]. For operation in DCM, the duty-ratio constraint d_2 is also derived as a function of terminal variables and the averaged inductor current. Based on the accuracy of portraying the high-frequency dynamics [60], the reduced-order [61] and the full-order [62], [63] models have been developed in the literature for ideal switching cells. In Fig. 8(b), the encircled part (cpa) is the general full-order equivalent cell for the ideal switched-inductor-cell [63]. Significant

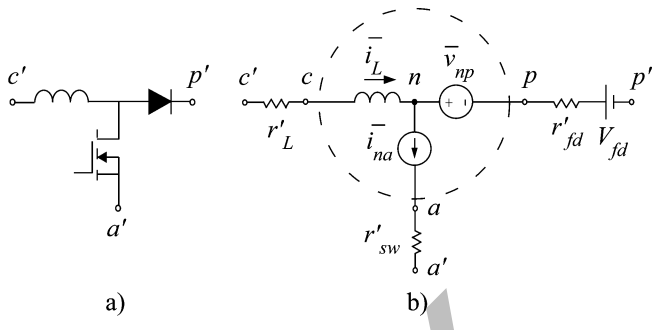

Fig. 8. Switched-inductor cell and its averaged equivalent circuit-model that includes dependent sources and parasitics.

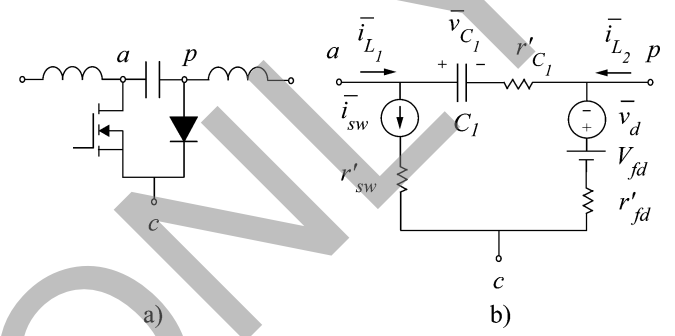

Fig. 9. Switched-capacitor cell and its averaged equivalent circuit-model that includes dependent sources and parasitics.

effort has also been made to include the effects of conduction losses [64]–[68]. In general, the modified parasitics are placed around the ideal components, as seen in Fig. 8(b), resulting in the averaged-switch model for the non-ideal cell [69]. The values of parasitics in the equivalent averaged cell of Fig. 8(b) are modified to account for the mode of operation and are generally different from the actual values of parasitics.

The average model for the switched-capacitor-cell of Fig. 9(a) may be obtained similar to the switched-inductor cell. The final full-order model accounting for parasitics is illustrated in Fig. 9(b) [70]. This equivalent averaged cell is also very general as it reduces to a simpler one if the parasitics are neglected. Circuit implementation and state-variable implementation of the switched-capacitor converters can be found in [70].

B. State-Space Averaging of DC–DC Converters

In the state-space averaging method, the state equations are obtained for each topology within a switching interval T_s (see Fig. 4) [57], [58]. The final average model is then composed of the weighted sum of the state-space equations for different subintervals. The corrected full-order state-space averaged model [63] for ideal converter is then of the form

$$\dot{\bar{\mathbf{x}}} = \left(\sum_{k=1}^{3} d_k \, \mathbf{A}_k\right) \mathbf{M}\, \bar{\mathbf{x}} + \left(\sum_{k=1}^{3} d_k \mathbf{B}_k\right) \mathbf{u} \qquad (2)$$

where corresponding state vector $\bar{\mathbf{x}}$ includes the inductor currents and capacitor voltages, and $\mathbf{M}$ is the so-called correction matrix. The diagonal matrix $\mathbf{M}$ needs to be added in the above equation to make the model properly work in DCM. For CCM operation, matrix $\mathbf{M}$ is simply set to identity. For DCM, the

elements of $\mathbf{M}$ depend on the duty cycle d_1, which is determined externally, and the duty ratio constraint d_2, which is algebraically-dependent on other system variables. If parasitics are included, the so-called piecewise linear approximation for the inductor current [58], [59], [63], [71], [72] does not hold [73] and the peak value of inductor current also changes (see Fig. 1 in [74]). Unlike the ideal case, it is then very difficult to evaluate the correction matrix analytically [75]. It can be shown that the averaged state-space model can be rewritten in a more general form [75]

$$\dot{\bar{\mathbf{x}}} = \left(\sum_{k=1}^{3} d_k \mathbf{A}_k \mathbf{W}_k\right) \bar{\mathbf{x}} + \left(\sum_{k=1}^{3} d_k \mathbf{B}_k\right) \mathbf{u} \tag{3}$$

that can account for arbitrary parasitics and possible nonlinearity of the current/voltage waveforms. The formulation (3) does not rely on small- and/or linear-ripple approximation and is therefore more general than (2). However, analytical derivation of the weighing-correction matrices $\mathbf{W}_k(d_1, \bar{i}_L)$ may be challenging, and as an alternative methodology these functions may be calculated numerically for a desired range of operating conditions [75].

C. Average-Value Modeling of DC–AC Converters

To demonstrate dynamic average modeling of dc-ac converters, let us first consider the voltage-source inverter based on the switch network of Fig. 2(b). In many power applications, the efficiency of converters is quite high and therefore the conduction losses are often neglected in analysis of transients. As described earlier, the ac variables must be expressed in an appropriate reference frame. Typically, the so-called converter reference frame [56], in which the d -axis component of the voltage is identically zero, is chosen to facilitate the analysis. The relationship between the converter and arbitrary reference frames may be deduced according to Fig. 10 as:

$$\begin{bmatrix} v_{qs}^{c} \\ 0 \end{bmatrix} = \begin{bmatrix} \cos(\phi_c) & \sin(\phi_c) \\ -\sin(\phi_c) & \cos(\phi_c) \end{bmatrix} \begin{bmatrix} v_{qs}^{a} \\ v_{\mathrm{ds}}^{a} \end{bmatrix}. \tag{4}$$

Depending on the converter topology and application of the required model, the dynamic average-value model can be structured in the form of equivalent circuits shown in Fig. 11. Since the switching cells of Fig. 2 do not contain any energy storage components, the voltages and currents on the ac side can be related to the dc side variables through functions that are purely algebraic [76]. This approach lands itself on implementation depicted in Fig. 11(a). In particular, the voltages on the ac side and dc link are related as follows:

$$\|\bar{\mathbf{v}}_{qds}\| = \alpha(\cdot)\bar{v}_{\mathrm{dc}} \tag{5}$$

where $\alpha(\cdot)$ is an algebraic function. The dc bus current may also be expressed in the following form:

$$\bar{i}_{\mathrm{dc}} = \beta(\cdot)\|\bar{\mathbf{i}}_{qds}\| \tag{6}$$

where $\beta(\cdot)$ is another algebraic function. Both $\alpha(\cdot)$ and $\beta(\cdot)$ depend on the type of inverter and its operating/loading conditions.

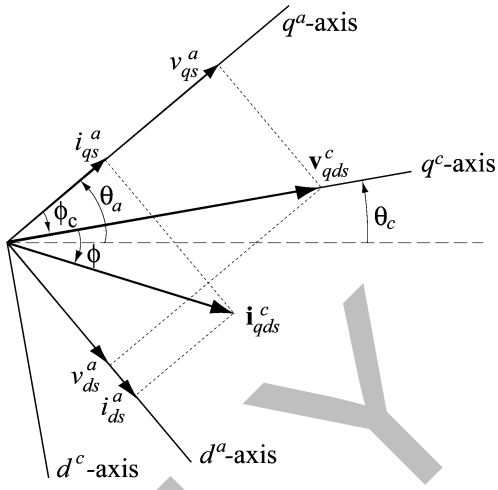

Fig. 10. Relationship between converter and arbitrary reference frames.

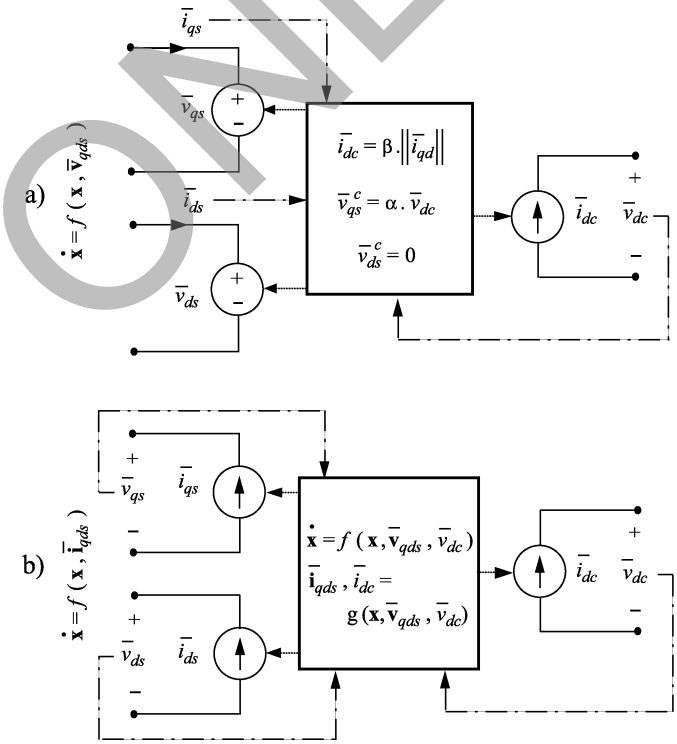

Fig. 11. Average-value models for the voltage source inverter: (a) using algebraic-parametric functions relating ac and dc variables; and (b) using a state model for representing effective commutating and/or dc-filter inductances.

Functions (5) and (6) can be established by applying the energy conservation principle to the converter cell. In particular, looking at the ac side, the three phase power can be written as

$$P = \frac{3}{2}\|\bar{\mathbf{v}}_{qds}\|\|\bar{\mathbf{i}}_{qds}\|\cos\phi \tag{7}$$

where ϕ is the power factor angle. Assuming an ideal (lossless) converter, the power calculated using (7) is equal to the power on the dc link. Therefore, the dc bus current can be written as follows:

$$\bar{i}_{\mathrm{dc}} = \frac{P}{\bar{v}_{\mathrm{dc}}} = \left(\frac{3}{2}\alpha(\cdot)\cos\phi\right)\|\bar{\mathbf{i}}_{qds}\|. \tag{8}$$

TABLE I
ALGEBRAIC FUNCTIONS FOR COMMON VOLTAGE-SOURCE INVERTERS

Function	Six Step Inverter	Six-Step PWM	Sine-Triangle/ Space-Vector Modulation
α	$\frac{2}{\pi}$	$\frac{2}{\pi}d$	$\frac{1}{2}d$
β	$\frac{3}{\pi}\cos\phi$	$\frac{3}{\pi}d\cos\phi$	$\frac{3}{4}d\cos\phi$

Finally, comparing (8) and (6), $\beta(\cdot)$ is obtained as

$$\beta(\cdot) = \frac{3}{2}\alpha(\cdot)\cos\phi. \tag{9}$$

Since the angle ϕ depends on the load, the value of $\beta(\cdot)$ also depends on loading conditions. Based on Fig. 10, the angle ϕ may be expressed in terms of the qd components of the voltage and current as

$$\phi(\cdot) = \tan^{-1}\left(\frac{\overline{i}^a_{\rm ds}}{\overline{i}^a_{qs}}\right) - \tan^{-1}\left(\frac{\overline{v}^a_{\rm ds}}{\overline{v}^a_{qs}}\right). \tag{10}$$

In the following discussion, the PWM-controlled VSI with the two-level topology depicted in Fig. 2(b) is considered. Average modeling of three- and four-level converters has been set forth in [77] and [78], respectively. The values of parametric functions $\alpha(\cdot)$ and $\beta(\cdot)$ for several commonly-used modulation strategies (i.e., basic six-step, PWM, sine-triangle, and space-vector) [56] are summarized in Table I. The corresponding average-value model is shown in Fig. 11(a), which assumes that the dc-link voltage is available (which is typically the case due to a large capacitor in dc-link) and that the ac-side is connected to an inductive network (e.g., electric machine). If the state-variable approach is used, the inductive network typically requires input voltages $\overline{\mathbf{v}}_{qds}$. Therefore, the ac-side voltages become the output of the converter AVM and are calculated in terms of the dc bus voltage using (5) and the function $\alpha(\cdot)$. A coordinate transformation may be used to re-calculate these voltages from the converter reference frame to the physical variables for interfacing with the external inductive network [56]. The ac side currents $\overline{\mathbf{i}}_{qds}$ are calculated by the external network and become the input for the converter AVM. Finally, the current $\overline{i}_{\rm dc}$ that is injected into the dc bus is calculated using (6) and the function $\beta(\cdot)$.

The methodology to develop an average model for the line-commutated converter of Fig. 2(a) has similar foundation. In general, obtaining the above-mentioned algebraic functions is more challenging in this case due to the complicated switching pattern and the existence of several operational modes as explained in Section II.B. In particular, the discontinuity of stator currents and the dependency of conduction/commutation times on the dynamic state of the network require special considerations. The available models for this class of converters are summarized in Table II. These models can be broadly classified based on whether they are fed from a voltage source or a rotating machine, as well as the pulse count (number of phases).

TABLE II
AVERAGE-VALUE MODELS FOR LINE COMMUTATED CONVERTERS

	Voltage Source	Machine-Converter
Three-phase	[56], [79]–[82]	[76], [83]–[88]
Five-phase	[89], [90]	[89], [90]
Six-phase	[51], [91], [92]	[93]–[95]
Nine-phase	[80], [81], [96], [97]	–

Several analytically-derived AVMs have been proposed in the form of the equivalent circuit shown in Fig. 11(b). The approach requires careful averaging of the transformed qd currents/voltages inside the conduction and commutation subintervals, respectively, and then adding the result to find the accurate average values over the entire switching interval T_s. The averaged ac variables are then related to the dc-link variables. A reduced-order average-value model is developed in [56], where the dynamics of the dc bus are partly neglected within the switching interval. This formulation allows the presence of commutating inductances on the ac side as well as the dc filter inductance. The dynamics of these two inductances are combined into one first-order state model that is represented as a block in Fig. 11(b). Due to such model structure, it has input voltages $\overline{\mathbf{v}}_{qds}$ and $\overline{v}_{\rm dc}$, and output currents $\overline{\mathbf{i}}_{qds}$ and $\overline{i}_{\rm dc}$. An effort has been made in [80] and [81] to improve the accuracy of this type of models by assuming linear (1st order) dynamics for the dc current within the switching interval instead of constant $i_{\rm dc}$ as has been done in [56]. Most analytically-derived models for the line-commutated converters assume only one operating mode based on conduction/commutation subintervals (2–3 mode discussed in Section II.B). In general, the average models may be obtained individually for all possible operating modes. If this has been achieved, the final model should be implemented such that these sub-models are switched on the fly as the converter operating mode changes during transients.

The development of dynamic average model becomes more difficult when instead of voltage source, as in [56], the converter is fed from a rotating machine. In this case, the effective commutating inductance changes with the rotor position (e.g., salient pole synchronous machine). Both reduced- and full-order models can be found in [83]–[85]. The general property of such analytically-derived models is that they result in implicit transcendental equations that internally require iterative (numerical) solution at each time step. A computer-aided approach has been proposed in the literature for the line-commutated converters to simplify the model development [76]. Therein, the parametric functions $\alpha(\cdot)$ and $\beta(\cdot)$ are established numerically for a wide range of operating conditions to cover all

possible operating modes. Once the functions $\alpha(\cdot)$ and $\beta(\cdot)$ are established, the final model may be formulated as the circuit shown in Fig. 11(a).

Converters with higher pulse-count include 12-, 18-, and 24-pulse configurations, which are generally considered to improve the quality of dc voltage and current at the output as well as the harmonic contents of the ac current at the input. The complexity of operational modes increases as the number of pulses increase making the average-value modeling more challenging [51], [52]. Analytical models have been developed in [80], [81] for the 18- pulse rectifier in mode 1. Computer-aided approaches have been used in [94], [95] to develop average-value models for 12- pulse rectifiers.

IV. Application to Large-Signal Time-Domain Analysis

Regardless of the method used to develop the dynamic average model, it generally should preserve the system-level behavioral characteristics of the original system with switching that is captured by the detailed model. To better understand the features and potential benefits of dynamic average modeling, it is instructive to first discuss the simulation packages that are commonly-used to analyze the transients in power and power-electronic systems. These software packages may be broadly categorized into nodal-analysis-based [1]–[5], and state-variable-based [6]–[12] programs.

A. Electromagnetic Transient Programs

The list of programs based on nodal analysis [98], [99] (or modified nodal analysis) includes EMTP-type and Spice-type programs [100]. The underlying solution approach is based on discretizing the differential equations for each circuit component using a particular integration rule. The EMTP [99] uses an implicit trapezoidal rule for discretization and formulating the network nodal equation that has the following general form:

$$\mathbf{G}\mathbf{V}_n = \mathbf{I}_h. \tag{11}$$

Here, $\mathbf{G}$ is the network nodal conductance matrix, and the vector $\mathbf{I}_h$ includes the so-called history current sources and independent sources injected into the nodes. The nodal voltages $\mathbf{V}_n$ are unknown and calculated by solving (11) at every time step. As the $\mathbf{G}$ matrix is usually sparse, specially designed techniques such as optimal reordering schemes and partial LU factorization [101], [102] are often used to solve this linear system instead of inverting the matrix $\mathbf{G}$ directly.

In a typical EMTP formulation which uses a fixed time-step Δt, topological changes due to switching events require special consideration since such changes may happen inside a time-step. A trivial solution is to reduce the step size until a sufficient accuracy of solution is achieved. This would result in using very small time steps and increase the computational burden of the overall simulation. Significant effort has been made to design efficient algorithms for handling switching events [103]–[108]. Such methods typically include interpolation and/or extrapolations within a time step.

Fig. 12 shows the time-stepping procedure in a typical EMTP. After the initialization, the simulation enters the major time-stepping loop which continues to execute until the end of simulation when the t_{final} is reached. In each time-step, the network

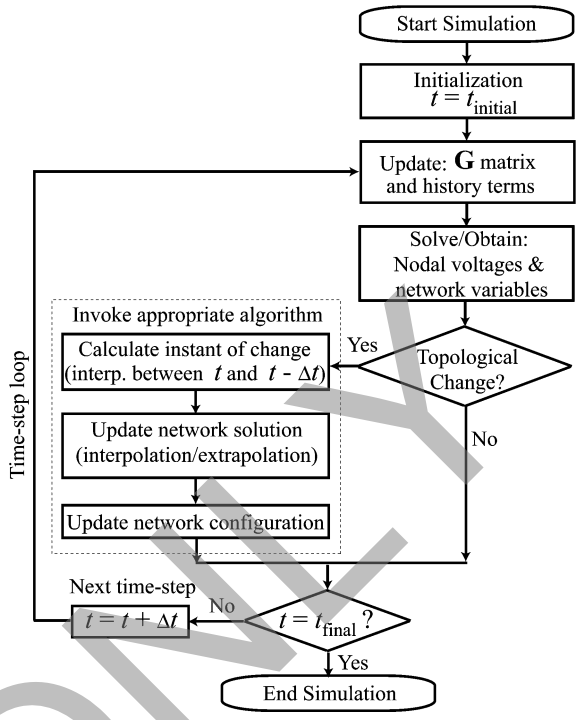

Fig. 12. Flowchart of a typical nodal-analysis-based solver.

G matrix and history terms are updated as needed, the nodal equations are solved, and the nodal voltages are calculated.

At each time step, the network variables are computed to perform the test for the changes in topology. If a change in topology within a given time step is detected (turning on/off of a diode, thyristor, transistor, etc.), the present time step is not accepted and a special algorithm has to be evoked. A typical algorithm interpolates between the solution points to precisely locate the time instance of the switching event within the time-step. Then, the network equation has to be solved considering the shorter subinterval before the switching instance. After that, the system is updated for the new topology and is solved again. For re-synchronizing back with the existing time step, several solutions have been proposed in the literature using interpolation/extrapolation [103], [105], [107]–[109]. In many EMTP languages, the so-called Critical Damping Algorithm (CDA) [110], [111] is invoked to suppress the artificial numerical oscillations due to the insufficient damping of the trapezoidal integration. This procedure is then applied whenever there is a switching in the system until the end of simulation.

B. State Variable-Based Simulators

State Variable (SV) approach is also used for analysis of dynamic systems including electric power systems. The examples of software packages include ACSL [6], Easy5 [7], Eurostag [8], and the well-known MATLAB \ Simulink [9]. There are also more specialized tools such as SimPowerSystems (SPS) [10], PLECS [11], and ASMG [12], etc., that come with circuit interfaces and built-in libraries for simulation of transients in power and power-electronic modules [112]. Internally, the program engine assembles system of differential and/or differential algebraic equations (DAEs) that constitute the state-variable-based

model of the overall system. Depending upon the features of a given program, the DAEs may be converted into a first-order system of differential equations (ODE) as

$$\begin{aligned}\dot{\mathbf{x}} &= \mathbf{f}(\mathbf{x}, \mathbf{u}, t)\\ \mathbf{y} &= \mathbf{g}(\mathbf{x}, \mathbf{u}, t)\end{aligned} \tag{12}$$

where $\mathbf{x}$ is the vector of state variables; $\mathbf{u}$ is the vector of inputs; t is a scalar to denote time; and $\mathbf{y}$ is the vector of outputs. Whenever appropriate, the linear time invariant part of the system/circuit may then be represented using a more compact state-space equation

$$\begin{aligned}\dot{\mathbf{x}} &= \mathbf{A}\mathbf{x} + \mathbf{B}\mathbf{u}\\ \mathbf{y} &= \mathbf{C}\mathbf{x} + \mathbf{D}\mathbf{u}\end{aligned} \tag{13}$$

where $\mathbf{A}, \mathbf{B}, \mathbf{C}$, and $\mathbf{D}$ are the so-called state-space matrices that are computed for the given topology and parameters of the linear circuit. In some tools, for example SimPowerSystems [10], the circuit part is directly implemented in the form of (13), whereas the remaining parts of the system (e.g., control blocks, mechanical subsystem, etc.) are in the more general form of (12).

The time-domain transient responses are then calculated numerically by integrating the state-space model (12)–(13) using either fixed- or variable-step ODE solvers embedded in the SV program. The formulations (12)–(13) also contain very useful information about the system's dynamical modes which is often utilized together with numerical linearization for the frequency-domain characterization and design of controllers.

Unlike EMTP-based simulators, the SV-based programs allow the use of variable-step integration (solvers) where the step-size is dynamically adjusted to satisfy the local accuracy constraints. Fig. 13 shows a typical time-stepping flowchart of the SV-based programs. As usual, after initialization the program estimates the size for the first time step and the simulation enters the major time-stepping loop.

The step-size is limited between the user-defined minimum and maximum values of $\Delta t_{\min}$ and $\Delta t_{\max}$, respectively. In the next step, the state vector $\mathbf{x}_{n+1}$ is computed together with an error function estimate $\mathbf{r}$ and the vector of output variables $\mathbf{y}_{n+1}$. The local accuracy of the solution in each time-step is assessed based on the value of this error function. Typically, the user can also specify the absolute and relative error tolerances. If the error estimate $\mathbf{r}$ exceeds either of the tolerances, the time-step is reduced (for example to a half of the previous Δt) and the solver attempts the solution again. To accurately handle the switching discontinuities, the algorithm also computes a special vector of event variables $\mathbf{e}_{n+1}$. These variables are monitored at each time step for zero-crossing. A topological change in the system is detected whenever one of the variables in $\mathbf{e}_{n+1}$ changes the sign within the time step. If this condition is detected, the time step is reduced and the solution iterates inside the minor time-stepping loop to precisely locate the zero-crossing. After that, the equations are updated accordingly and the simulation proceeds. Hence, very frequent switching will result in more iterations and effective reduction of the time step. This may lead to a significant increase in the computation time especially when a large number of switches are present in the network or a high frequency switching is taking place.

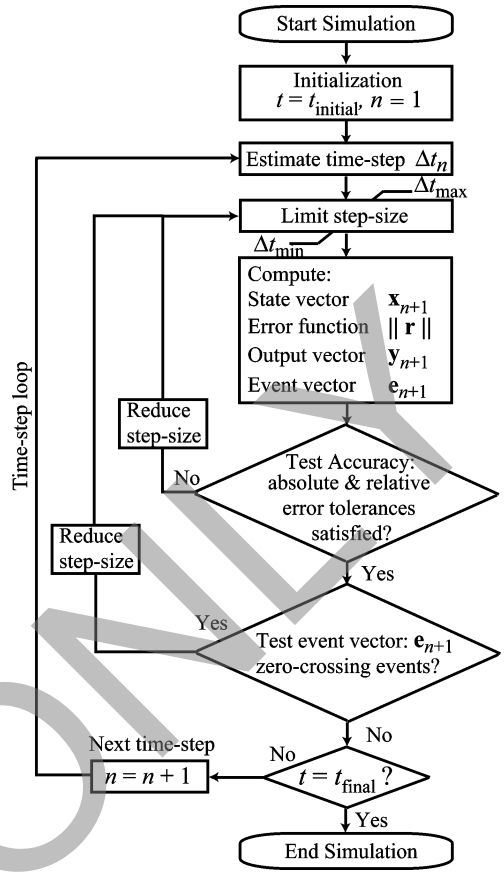

Fig. 13. Flowchart of a typical variable-step state-variable-based solver.

In time-domain studies, the transient behavior of the system may be predicted with desired accuracy using the dynamic average models. Since the averaging, as defined by (1), removes switching ripple, the resulting AVMs generally do not have previsions to predict any switching-harmonic-related phenomena. However, in dynamic sense, such models should be valid in the low frequency range up to and approaching the switching frequency of the converter. Dynamic average models do not include electronic switching, which often requires the use of small time step size and increases the computational burden for either the EMTP or the SV solution approach as explained above (see Figs. 12 and 13). The dynamic AVMs are continuous (although may be nonlinear) and can use much larger time steps and therefore typically execute orders of magnitude faster than the corresponding detailed switching models. This can be particularly important for system-level transient studies where the overall system may include a large number of power-electronic modules.

V. Application to Small-Signal Frequency-Domain Analysis

The small- and large-displacement analyses are important tools for assessing the stability of power-electronics-based systems and design of corresponding controllers. Many conventional stability criteria rely on impedance characteristics and

input-output transfer functions [113], [19]. Such small-signal characteristics can be extracted from the hardware (which is very expensive and is not always possible) or from the detailed switch-level model of the system (which can be done at the design stage) using the frequency-sweep method and similar techniques [114]. However, using the detailed models directly for extracting the impedances and transfer functions becomes a time consuming and challenging procedure especially when many data point are required at low frequency.

To illustrate the approach based on the small-signal impedances, let us first consider a dc-dc converter connected between System 1 and System 2 as shown in Fig. 14(a). Assume that this converter is operating in a steady-state determined by the fixed control input duty cycle $d = D$ and input voltage $v_{\rm in} = V_{\rm in}$. A small-signal perturbation is then considered around this operating point, i.e., the small-signal voltage $\hat{v}_{\rm in}$ which is much smaller in amplitude compared to the quiescent value $V_{\rm in}$ is injected at the input. This small-signal injection is going to introduce a small perturbation in other network variables about their quiescent operating points. The small-signal input impedance $Z_{\rm in}$ of the dc-dc converter may then be written as

$$Z_{\rm in}(s) = \frac{\hat{v}_{\rm in}(s)}{\hat{i}_{\rm in}(s)}. \tag{14}$$

The frequency of the injection signal may be slowly swept in the desired frequency range and in each point the magnitude and phase of the impedance are obtained based on (14). This impedance is also the impedance of System 2 as mapped through the switching cell of the dc-dc converter. Therefore, the impedance $Z_{\rm in}$ will depend on the dynamics of System 2 and the properties of the switching converter itself, e.g., switching strategy, modulation, controls, etc. Similarly, if the small-signal injection is performed at the output of the converter, the output impedance $Z_{\rm out}$ is calculated as

$$Z_{\rm out}(s) = \frac{\hat{v}_{\rm out}(s)}{\hat{i}_{\rm out}(s)} \tag{15}$$

which is the equivalent impedance of the System 1 as seen through the switching network of the converter.

If the input voltage is kept constant, and the small-signal perturbation $\hat{d}$ is considered in the control input, the control-to-output transfer function of the dc-dc converter $H(s)$ may be defined as

$$H(s) = \frac{\hat{v}_{\rm out}(s)}{\hat{d}(s)} \tag{16}$$

where $\hat{v}_{\rm out}$ is the small-signal perturbation in the output voltage due to the changes in the control input $\hat{d}$.

The small-signal impedance-based analysis also extends to the ac-dc converters [19], [115]–[120]. To illustrate this, let us now consider the ac-dc converter connected between System 1 and System 2 as shown in Fig. 14(b). Similarly, the system has to operate in a steady state for the analysis to be valid. Thereafter, the small-signal impedance from the dc side may be expressed as

$$Z_{\rm dc}(s) = \frac{\hat{v}_{\rm dc}(s)}{\hat{i}_{\rm dc}(s)}. \tag{17}$$

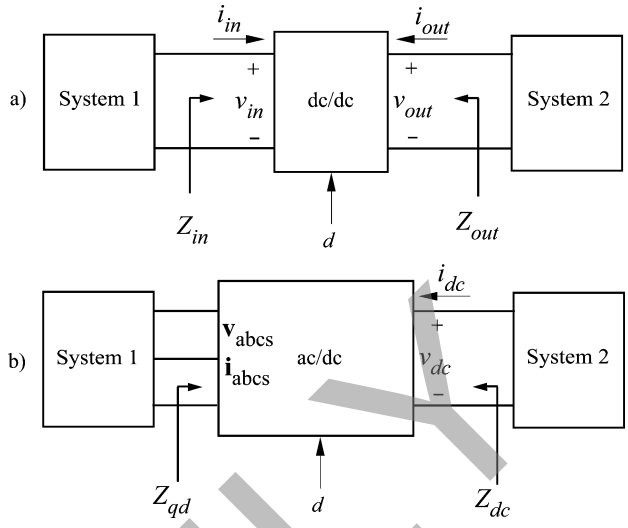

Fig. 14. System-level impedance-based representation of subsystems: (a) the subsystems are interconnected through dc-dc converter; and (b) the subsystems are interconnected through ac-dc converter. The variable d is used here to denote the duty cycle.

This impedance looking from the dc side is determined by the converter and the three phase ac System 1 as seen through the converter switching cell.

Evaluating impedance of the system looking from the ac side requires special consideration because the ac variables are inherently time-variant even in steady state. To extend the impedance-based approach to the ac systems, the ac variables have to be viewed in a system of coordinates where they appear constant in steady state. This extension has been made in [19], where this approach was developed for the stability analysis of ac-dc electric power systems. Therefore, the physical variables on the ac side, $\mathbf{v}_{abcs}$ and $\mathbf{i}_{abcs}$, are transferred into a synchronous reference frame. The resulting variables $\mathbf{v}_{qds}$ and $\mathbf{i}_{qds}$ have the required property of being constant in steady state. For this reason, the appropriate impedances (as well as the averaging) are expressed in terms of these transformed variables. Specifically, assuming that the system operates in a steady state operating point determined by the external inputs and control signal d, the small-signal perturbations can be applied. Neglecting the zero sequence, there are two axes to be considered for calculating the appropriate impedance on the ac side denoted here by $\mathbf{Z}_{qd}$. For example, a small-signal perturbation $\hat{v}_{qs}$ is first considered around the steady-state value V_{qs}. The response of the system in terms of currents generally will be seen in both q and d axes, respectively. This will give the first row of the transfer matrix (18). Next, a small-signal perturbation $\hat{v}_{ds}$ is considered around V_{ds}. Similarly, the system response in terms of currents will be seen in both axes. Calculating these transfer functions will give the second row of the impedance transfer matrix $\mathbf{Z}_{qd}$. The final form of impedance transfer matrix is therefore

$$\mathbf{Z}_{qd} = \begin{bmatrix} Z_{qq} & Z_{qd} \\ Z_{dq} & Z_{dd} \end{bmatrix} = \begin{bmatrix} \left.\frac{\hat{v}_q(s)}{\hat{i}_q(s)}\right|_{\hat{v}_d=0} & \left.\frac{\hat{v}_q(s)}{\hat{i}_d(s)}\right|_{\hat{v}_d=0} \\ \left.\frac{\hat{v}_d(s)}{\hat{i}_q(s)}\right|_{\hat{v}_q=0} & \left.\frac{\hat{v}_d(s)}{\hat{i}_d(s)}\right|_{\hat{v}_q=0} \end{bmatrix}. \tag{18}$$

On the one hand, the transfer function characteristics (14)–(18) can be calculated using the detailed switching models of the overall system depicted in Fig. 14. However, since the detailed models are computationally intensive, determining the impedance over a wide range of frequencies is a very time consuming procedure, particularly when obtaining data points at very low frequencies (<10 Hz).

On the other hand, extracting the above-mentioned frequency-domain characteristics from the dynamic average models in either EMTP- or SV-based simulation software has many advantages. In the case of nodal-analysis-based simulators, the frequency sweep methods become more effective since the averaged models do not have switching and can execute faster. However, if the SV approach is used, then the required small-signal characteristics can be obtained almost immediately. Since the AVMs are continuous and time-invariant in steady state, the well-known linearization techniques may be employed to obtain a small-signal model about any desired operating point. In particular, the dynamic AVM will typically have the form of (12). Assuming a small-signal perturbation about the steady-state operating point as

$$\begin{aligned} \mathbf{x} &= \mathbf{X} + \hat{\mathbf{x}} \\ \mathbf{u} &= \mathbf{U} + \hat{\mathbf{u}} \end{aligned} \tag{19}$$

where $\hat{\mathbf{x}}$ and $\hat{\mathbf{u}}$ are small-signal disturbances about the operating point values $\mathbf{X}$ and $\mathbf{U}$, the linearized equations are then obtained as

$$\begin{aligned} \dot{\hat{\mathbf{x}}} &= \frac{\partial \mathbf{f}(\mathbf{X},\mathbf{U},t)}{\partial \mathbf{x}}\hat{\mathbf{x}} + \frac{\partial \mathbf{f}(\mathbf{X},\mathbf{U},t)}{\partial \mathbf{u}}\hat{\mathbf{u}} = \hat{\mathbf{A}}\hat{\mathbf{x}} + \hat{\mathbf{B}}\hat{\mathbf{u}} \\ \hat{\mathbf{y}} &= \frac{\partial \mathbf{g}(\mathbf{X},\mathbf{U},t)}{\partial \mathbf{x}}\hat{\mathbf{x}} + \frac{\partial \mathbf{g}(\mathbf{X},\mathbf{U},t)}{\partial \mathbf{u}}\hat{\mathbf{u}} = \hat{\mathbf{C}}\hat{\mathbf{x}} + \hat{\mathbf{D}}\hat{\mathbf{u}} \end{aligned} \tag{20}$$

which has the form of (13). Once the state-space matrices $\hat{\mathbf{A}}, \hat{\mathbf{B}}, \hat{\mathbf{C}}$, and $\hat{\mathbf{D}}$ of the linearized system are calculated, obtaining any transfer function of the system becomes a straightforward procedure. In a very general case, the input-output transfer function matrix $\mathbf{H}(s)$ (considering all inputs and outputs) may be written as

$$\mathbf{H}(s) = \hat{\mathbf{C}}(s\mathbf{I} - \hat{\mathbf{A}})^{-1}\hat{\mathbf{B}} + \hat{\mathbf{D}}. \tag{21}$$

A subset of (21) will contain any particular transfer functions (impedances) (14)–(18). In most SV-based simulation packages, such as [9], this procedure can be done automatically which becomes a powerful tool for system-level analysis and design of controllers.

VI. Example System

To demonstrate the properties and benefits of the average-value models, in this paper we consider a micro-wind turbine generator system depicted in Fig. 15. Such systems may be used to generate power for telecommunication equipment in the remote areas where an electric grid may not be easily accessible. A typical low-cost system consists of a wind turbine coupled to a Permanent Magnet Synchronous Machine (PMSM) through a gearbox. The generator feeds a rectifier circuit, followed by an L-C filter, and a dc-dc converter which is connected to the dc bus. The controller adjusts the duty-cycle and regulates the output voltage to the appropriate level, typically 28 V dc. This system contains mechanical components, rotating machine, line-commutated ac-dc converter, dc-dc converter, and a controller; and is therefore considered a suitable example.

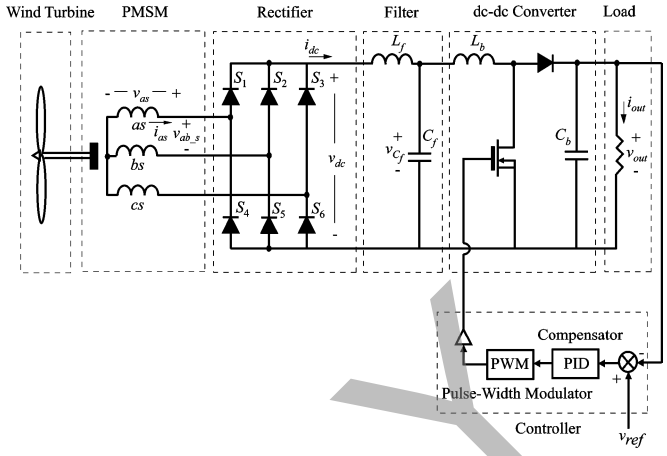

Fig. 15. Example PMSM micro-wind turbine generator system.

A. Large-Signal Time-Domain Analysis

The example system is modeled in detail considering the switching of all diodes and transistor. The average-value model has been then developed using the methodology described in Sections III.C and III.A, for the machine-converter and the dc-dc converter, respectively. In the computer study considered in this section, the micro-turbine system is subjected to the speed change shown in Fig. 16 (top plot). The transient responses as observed in the output voltage, output current, dc-link capacitor voltage, and the duty cycle are also shown in Fig. 16. It is observed that the average-value model predicts the behavior of the detailed model very accurately.

The computer studies were carried out using MATLAB\Simulink software run on a personal computer (PC) with 2.4 MHz AMD 3800+ processor. To give the reader a better idea on how effective the AVM can be, the detailed and average-value models are compared further. To achieve accurate results with the detailed model it was found that the variable-step solver ODE23 with maximum allowable time step of 1e-5s was needed. The absolute and relative error tolerances were both set to 1e-4. To obtain the results of Fig. 16, the detailed simulation took 121s of CPU time requiring a total of 386680 time-steps. Relatively small time steps were required in order to capture all the switching events due to high frequency switching of the boost converter as well as the switching of the rectifier diodes. However, the AVM does not have switching and can be executed with much larger time steps. With the same tolerances of 1e-4 and the maximum allowable time step of 1e-2, using the same variable-step solver, the AVM simulation took 0.062s of CPU time requiring only 625 time-steps in total. This demonstrates

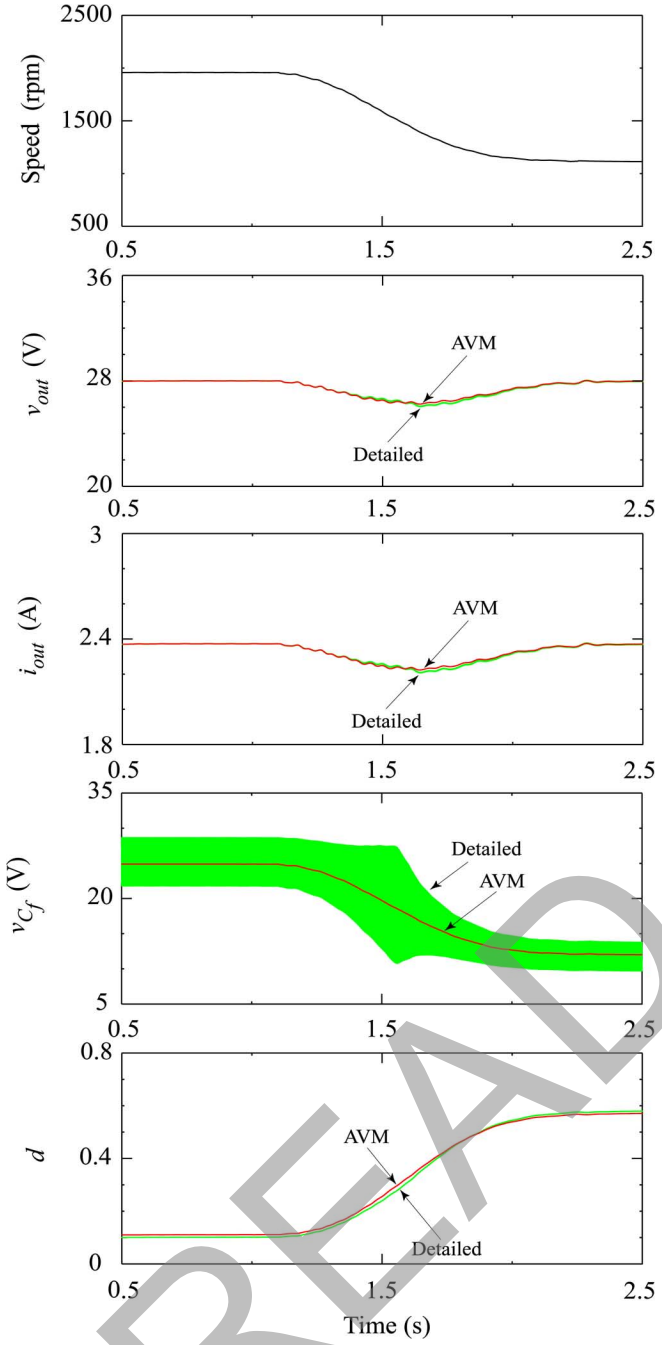

Fig. 16. Waveforms of the example PMSG micro-wind turbine generator system.

an increase of simulation efficiency of 1951 times to obtain the results of Fig. 16.

B. Small-Signal Frequency-Domain Analysis

It is also desired to compare the detailed and average-value models in portraying the frequency-domain characteristics of the system. For this purpose, a small-signal analysis is performed around the steady-state operating point corresponding to the shaft speed of 1500 rpm. First, the control loop is removed and the duty ratio of the transistor gate signal is fixed to 0.35 to obtain the output voltage of 28 V on the dc bus. The

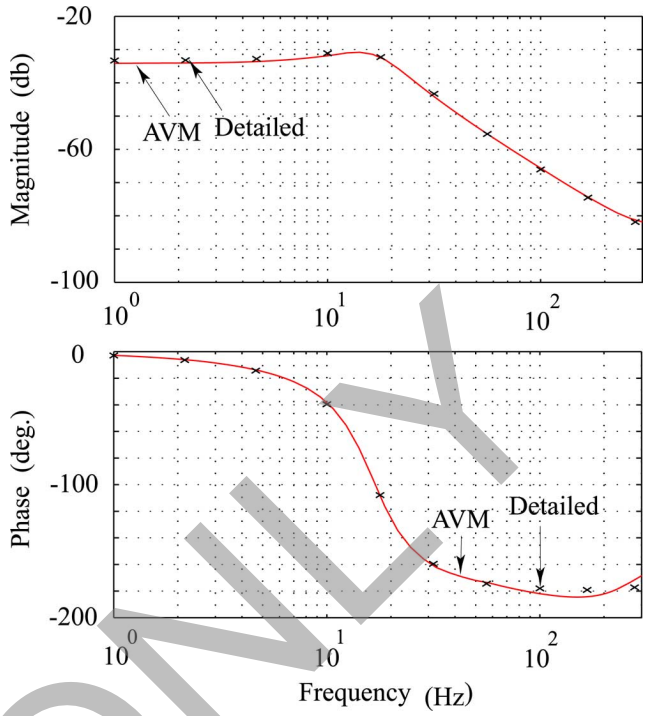

Fig. 17. Speed-to-output-voltage transfer function for the example system.

open-loop small-signal input-output transfer function $H(s)$ considered here is

$$H(s) = \frac{\hat{v}_{\text{out}}(s)}{\hat{n}(s)} \tag{22}$$

where $\hat{v}_{\text{out}}$ is the change in the output dc bus voltage due to the small signal perturbation in the shaft speed $\hat{n}$. This transfer function includes the effects of both ac-dc and dc-dc stages and is therefore a suitable measure of comparing the detailed and average-value models. This transfer function has been extracted using both models and the results are superimposed in Fig. 17. Since the input is the mechanical speed, lower frequency dynamics are of significant importance. Nevertheless, the results in Fig. 17 are illustrated for up to one-half of the lowest switching frequency present in the system, which corresponds to the diode rectifier stage (i.e., 300 Hz). As the switching frequency is approached further from this point, it would be normal to observe deviations between the results obtained from the detailed and average-value models. In the whole frequency range depicted in Fig. 17, however, the results demonstrate an excellent match between the detailed and average-value models.

VII. Concluding Remarks

This paper gives an overview of dynamic average-modeling techniques used to represent the static switching converters for system-level studies. The basic concepts and methodologies for developing and implementing average-value models of dc-dc as well as ac-dc converters are presented. The methodology of developing such models is based on averaging the variables (currents and voltages) within a switching interval and deriving the relationships that govern the dynamics of the system in terms of these averaged variables. An important property that is being achieved

through such derivations is that the averaged variables appear constant in steady state. To achieve this property for ac systems, the averaging has to be applied in a synchronous reference frame.

The resulting average models may have a number of useful applications. First of all, the averaged models are continuous and therefore can be solved using much larger time steps resulting in faster simulations. This feature can be useful for conducting large-signal time-domain transient studies of the systems with multiple power-electronic modules, controllers, and mechanical subsystems. Another application of averaged models is for the small-signal analysis, where the frequency-domain transfer functions and impedance characteristics are typically required for the design of controllers and stability analysis of the overall system. It has been shown that, once the dynamic average-value model is constructed, such small-signal characteristics can be rapidly obtained by means of numerical linearization. Overall, if derived and implemented correctly (with the understanding of limitations of the underlying averaging approach), the dynamic average-value models can be very powerful computational tools for large- and small-signal analysis of power and power-electronic systems.

An obvious limitation of the dynamic average-value modeling approach is that the phenomena associated with the switching harmonics are not considered on either ac or dc side. Therefore, it is important to keep in mind that the dynamic average model only approximates the original switching system in the range of low frequencies (typically approaching the switching frequency). This is due to the underlying principle of averaging the dc variables, or the transformed ac variables as viewed in qd synchronous reference frame, within a considered switching interval (window). Such averaging removes the effect of switching harmonics as well as puts the limit on the frequency range where such models can be considered useful and/or appropriate.

APPENDIX

A. PM Synchronous machine parameters:
3-phase, 2000 rpm, 8-pole,
$r_s = 0.22\,\Omega, \quad L_s = 0.37$ mH, $\lambda'_m = 21$ mV·s.
B. Closed-loop system parameters:
$C_f = 100\ \mu$F, $L_f = 0$ mH.
Boost Converter: $L_b = 11$ mH, $C_b = 4$ mF.
Controller: $k_p = 2, k_i = 65, V_{\rm ref} = 28$ V.
Pulse-Width Modulator: $V_m = 15$ V, $f_{\rm sw-PWM} = 8$ kHz.

REFERENCES

[1] *"MicroTran Reference Manual"* MicroTran Power System Analysis Corp., 1997. [Online]. Available: http://www.microtran.com

[2] *"Alternative Transients Programs"* ATP-EMTP, ATP User Group, 2007. [Online]. Available: http://www.emtp.org

[3] PSCAD/EMTDC Ver. 4.0 On-Line Help. Manitoba HVDC Research Centre and RTDS Technologies Inc., Winnipeg, MB, Canada, 2005.

[4] *"Electromagnetic Transient Program,"* EMTP RV, CEA Technologies, Inc., 2007. [Online]. Available: http://www.emtp.com

[5] *"Resistive Companion Modeling and Simulation for the Virtual Test Bed (VTB), Modeling Guide 2003,"* Univ. South Carolina. [Online]. Available: http://vtb.ee.sc.edu

[6] ACSLX, Advanced Continuous Simulation Language, User's Guide, Ver. 2.4 The AEgis Technologies Group, Inc., 2008. [Online]. Available: http://www.acslsim.com

[7] EASY5 Engineering Software for the Design, Analysis and Simulation. MSC SimEnterprise, Inc., 2008. [Online]. Available: http://www.msc-software.com

[8] *"EUROSTAG: Software for Simulation of Large Electric Power Systems, Tractebel Energy Engineering,"* 2008. [Online]. Available: http://www.eurostag.be and www.tractebel-engineering.com

[9] *"Simulink Dynamic System Simulation Software, Users Manual,"* MathWorks Inc., 2008. [Online]. Available: http://www.mathworks.com

[10] *"SimPowerSystems: Model and Simulate Electrical Power Systems, User's Guide,"* The MathWorks Inc., 2006. [Online]. Available: http://www.mathworks.com

[11] *"Piecewise Linear Electrical Circuit Simulation (PLECS), User Manual, Version 1.4, Plexim GmbH,"* 2008. [Online]. Available: www.plexim.com

[12] *"Automated State Model Generator (ASMG), Reference Manual, Version 2,"* P C Krause & Associates Inc., 2003. [Online]. Available: www.pcka.com

[13] B. R. Needham, P. H. Eckerling, and K. Siri, "Simulation of large distributed DC power systems using averaged modelling techniques and the saber simulator," in *Proc. IEEE Applied Power Electronics Conf. Expo.*, Feb. 1994, vol. 2, pp. 801–807.

[14] K. S. Tam and L. Yang, "Functional models for space power electronic circuits," *IEEE Trans. Aerosp. Electron. Syst.*, vol. 31, no. 1, pp. 288–296, Jan. 1995.

[15] J. R. Lee, H. H. Cho, S. J. Kim, and F. C. Lee, "Modeling and simulation of spacecraft power systems," *IEEE Trans. Aerosp. Electron. Syst.*, vol. 24, no. 3, pp. 295–303, May 1988.

[16] T. L. Skvareniana, S. Pekarek, O. Wasynczuk, P. C. Krause, R. J. Thibodeaux, and J. Weimer, "Simulation of a more electric aircraft power system using an automated state model approach," in *Proc. 31st Intersoc. Energy Conversion Engineering Conf.*, Aug. 1996, pp. 133–136.

[17] C. E. Lucas, E. A. Walters, J. Jatskevich, O. Wasynczuk, and P. T. Lamm, "A distributed heterogeneous simulation of a representative aircraft power system," presented at the SAE Power Systems Conf., Coral Springs, FL, Oct. 2002.

[18] J. Jatskevich, O. Wasynczuk, E. A. Walters, E. C. Lucas, and Ed. Zivi, "Real-time distributed simulation of a DC zonal electrical distribution system," presented at the SAE Power Systems Conf., Coral Springs, FL, Oct. 2002.

[19] M. Belkhayat, "Stability criteria for ac power systems with regulated loads," Ph.D. dissertation, Purdue University, West Lafayette, IN, 1997.

[20] A. Emadi, A. Khaligh, C. H. Rivetta, and G. A. Williamson, "Constant power loads and negative impedance instability in automotive systems: Definition, modeling, stability, and control of power electronic converters and motor drives," *IEEE Trans. Veh.Technol.*, vol. 55, no. 4, pp. 1112–1125, Jul. 2006.

[21] J. Morren, S. W. H. de Haan, P. Bauer, J. Pierik, and J. Bozelie, "Comparison of complete and reduced models of a wind turbine with doubly-fed induction generator," in *Proc. 10 Eur. Conf. Power Electronics and Applications*, Sep. 2003, pp. 1–10.

[22] J. G. Slootweg, S. W. H. de Haan, H. Polinder, and W. L. Kling, "General model for representing variable speed wind turbines in power system dynamics simulations," *IEEE Trans. Power Syst.*, vol. 18, no. 1, pp. 144–151, Feb. 2003.

[23] J. G. Slootweg, S. W. H. de Haan, H. Polinder, and W. L. Kling, "Modeling new generation and storage technologies in power system dynamics simulations," in *Proc. IEEE Power Eng. Soc. Summer Meeting*, Jul. 2002, vol. 2, pp. 868–873.

[24] J. G. Slootweg, H. Polinder, and W. L. Kling, "Representing wind turbine electrical generating systems in fundamental frequency simulations," *IEEE Trans. Energy Convers.*, vol. 18, no. 4, pp. 516–524, Dec. 2003.

[25] C. Abbey, J. Morneau, J. Mahseredjian, and G. Joos, "Modeling requirements for transient stability studies for wind parks," in *Proc. IEEE Power Eng. Soc. General Meeting*, Jun. 2006, pp. 1–6.

[26] H.-S. Ko, J. Jatskevich, G. Dumont, and G.-G. Yoon, "An advanced LMI-based-LQR design for voltage control of grid-connected wind farm," *Int. J. Elect. Power Syst. Res.*, vol. 78, no. 4, pp. 539–546, Apr. 2008.

[27] H.-S. Ko and J. Jatskevich, "Power quality control of hybrid wind power generation system using fuzzy-LQR controller," *IEEE Trans. Energy Convers.*, vol. 22, no. 2, pp. 516–527, Jun. 2007.

[28] A. Tabesh and R. Iravani, "Small-signal dynamic model and analysis of a fixed-speed wind farm—A frequency response approach," *IEEE Trans. Power Del.*, vol. 21, no. 2, pp. 778–787, Apr. 2006.

[29] F. Katiraei and R. Iravani, "Power management strategies for a microgrid with multiple distributed generation units," *IEEE Trans. Power Syst.*, vol. 21, no. 4, pp. 1821–1831, Nov. 2006.

[30] F. Katiraei, R. Iravani, and P. W. Lehn, "Small-signal dynamic model of a micro-grid including conventional and electronically interfaced distributed resources," *Inst. Eng. Technol. Gen., Transm. Distrib.*, vol. 1, no. 3, pp. 369–378, May 2007.

[31] A. Yazdani and R. Iravani, "A unified dynamic model and control for the voltage-sourced converter under unbalanced grid conditions," *IEEE Trans. Power Del.*, vol. 21, no. 3, pp. 1620–1629, Jul, 2006.

[32] D. Povh, "Modeling of FACTS in power system studies," in *Proc. IEEE Power Eng. Soc. Winter Meeting*, Jan. 2000, vol. 2, pp. 1435–1439.

[33] M. O. Faruque, V. Dinavahi, S. Santoso, and R. Adapa, "Review of electromagnetic transient models for non-VSC FACTS," *IEEE Trans. Power Del.*, vol. 20, no. 2, pt. 1, pp. 1065–1079, Apr. 2005.

[34] Y. Yang, M. Kazerani, and V. H. Quintana, "Current-source converter based STATCOM: Modeling and control," *IEEE Trans. Power Del.*, vol. 20, no. 2, pt. 1, pp. 795–800, Apr. 2005.

[35] S. Jiang, U. D. Annakkage, and A. M. Gole, "A platform for validation of FACTS models," *IEEE Trans. Power Del.*, vol. 21, no. 1, pp. 484–491, Jan. 2006.

[36] G. Zhang and Z. Xu, "Steady-state model for VSC based HVDC and its controller design," in *Proc. CSEE*, Jan. 2002, vol. 22, no. 1, pp. 17–22.

[37] A. Gole and V. K. Sood, "A static compensator model for use with electromagnetic transients simulation programs," *IEEE Trans. Power Del.*, vol. 5, no. 3, pp. 1398–1407, Jul. 1990.

[38] R. Teichmann, M. Malinowski, and S. Bernet, "Evaluation of three-level rectifiers for low-voltage utility applications," *IEEE Trans. Ind. Electron.*, vol. 52, no. 2, pp. 471–481, Apr. 2005.

[39] C. S. Lefebvre, A. M. Gole, J. Reeve, L. Pilotto, N. Martins, and S. Bhattacharya, "Working group on dynamic performance and modeling of DC systems and power electronics for transmission systems. Report on test systems for AC/DC interaction studies," *IEEE Trans. Power Del.*, vol. 10, no. 4, pp. 2027–2034, Oct. 1995.

[40] X. Jiang and A. M. Gole, "A frequency scanning method for the identification of harmonic instabilities in HVDC systems," *IEEE Trans. Power Del.*, vol. 10, no. 4, pp. 1875–1881, Oct. 1995.

[41] R. M. Brandt, U. D. Annakkage, D. P. Brandt, and N. Kshatriya, "Validation of a two-time step HVDC transient stability simulation model including detailed HVDC controls and DC line L/R dynamics," in *Proc. IEEE Power Eng. Soc. General Meeting*, Jun. 2006, pp. 1–6.

[42] J. Morren, S. W. H. de Haan, and J. A. Ferreira, "Model reduction and control of electronic interfaces of voltage dip proof DG units," in *Proc. IEEE Power Eng. Soc. General Meeting*, Jun. 2004, vol. 2, pp. 2168–2173.

[43] K. Strunz, "Developing benchmark models for studying the integration of distributed energy resources," in *Proc. IEEE Power Eng. Soc. General Meeting*, Jun. 2006, pp. 1–2.

[44] K. Seita, I. Takano, H. Nishikawa, and Y. Sawada, "A study of operation characteristics of UPFC type dispersed power supply system with FC, PV and EDLC by improved EMAP model," in *Proc. IEEE Power Systems Conf. Expo.*, Oct. 2004, vol. 1, pp. 289–294.

[45] F. Wang, S. Rosado, T. Thacker, and D. Boroyevich, "Power electronics building blocks for utility power system applications," in *Proc. 4th Int. Power Electronics and Motion Control Conf.*, Aug. 2004, vol. 1, pp. 354–359.

[46] K. Thorborg, *Power Electronics*. Englewood Cliffs, NJ: Prentice-Hall, 1988.

[47] J. Rodriguez, S. Bernet, B. Wu, J. O. Pontt, and S. Kouro, "Multilevel voltage-source-converter topologies for industrial medium-voltage drives," *IEEE Trans. Ind. Electron.*, vol. 54, no. 6, pp. 2930–2945, Dec. 2007.

[48] T. Larsson, A. Edris, D. Kidd, and F. Aboytes, "Eagle pass back-to-back tie: A dual purpose application of voltage source converter technology," in *Proc. IEEE Power Eng. Soc. General Meeting*, Jul. 2001, vol. 3, pp. 1686–1691.

[49] S. Alepuz, S. Busquets-Monge, J. Bordonau, J. Gago, D. Gonzales, and J. Balcells, "Interfacing renewable energy sources to the utility grid using a three-level inverter," *IEEE Trans. Ind. Electron.*, vol. 53, no. 5, pp. 1504–1511, Oct. 2006.

[50] R. M. Davis, *Power Diode and Thyristor Circuits*. Cambridge, MA: Cambridge Univ. Press, 1971.

[51] Y. Tzeng, N. Chen, and R. Wu, "Modes of operation in parallel-connected 12-pulse uncontrolled bridge rectifiers without an interphase transformer," *IEEE Trans. Ind. Electron.*, vol. 44, no. 3, pp. 344–355, Jun. 1997.

[52] J. Jatskevich, O. Wasynczuk, E. A. Walters, C. E. Lucas, S. D. Pekarek, and P. T. Lamm, "Automated identification of the operational modes of switched electric circuits," *SAE Trans. J. Aerosp.*, vol. 109, no. 1, pp. 955–961, Oct. 2000.

[53] S. Sanders and G. C. Verghese, "Synthesis of averaged circuit models for switched converters," *IEEE Trans. Circuits Syst.*, vol. 38, no. 8, pp. 905–915, Aug. 1991.

[54] P. T. Krein, J. Bentsman, R. M. Bass, and B. L. Lesieutre, "On the use of averaging for the analysis of power electronic systems," *IEEE Trans. Power Electron.*, vol. 5, no. 2, pp. 182–190, Apr. 1990.

[55] S. Sanders, J. M. Noworolski, X. Z. Liu, and G. C. Verghese, "Generalized averaging method for power conversion circuits," *IEEE Trans. Power Electron.*, vol. 6, no. 2, pp. 251–259, Apr. 1991.

[56] P. C. Krause, O. Wasynczuk, and S. D. Sudhoff, *Analysis of Electric Machinery and Drive Systems*, 2nd ed. Piscataway, NJ: IEEE Press/ Wiley, 2002.

[57] J. G. Kassakian, M. F. Schlecht, and G. C. Verghese, *Principles of Power Electronics*. Reading, MA: Addison-Wesley, 1991.

[58] R. W. Erickson and D. Maksimovi, *Fundamentals of Power Electronics*, 2nd ed. Norwell, MA: Kluwer, 2001.

[59] J. Sun, "Unified averaged switch models for stability analysis of large distributed power systems," in *Proc. Applied Power Electronics Conf.*, Feb. 2000, vol. 1, pp. 249–255.

[60] D. Maksimovi, "Computer-aided small-signal analysis based on impulse response of dc/dc switching power converters," *IEEE Trans. Power Electron.*, vol. 15, no. 6, pp. 1183–1191, Nov. 2000.

[61] R. Tymerski and V. Vorperian, "Generation, classification and analysis of switched-mode dc-to-dc converters by the use of switched-inductor-cells," in *Proc. IEEE Int. Telecommunication Energy Conf.*, Oct. 1986, pp. 181–195.

[62] J. Chen and K. D. T. Ngo, "Alternate forms of the PWM switch model in discontinuous conduction mode," *IEEE Trans. Aerosp. Electron. Syst.*, vol. 37, no. 2, pp. 754–758, Apr. 2001.

[63] J. Sun, D. M. Mitchell, M. F. Greuel, P. T. Krein, and R. M. Bass, "Averaged modeling of PWM converters operating in discontinuous conduction mode," *IEEE Trans. Power Electron.*, vol. 16, no. 4, pp. 482–492, Jul. 2001.

[64] D. Czarkowski and M. K. Kazimierczuk, "Energy-conversion approach to modeling PWM dc-dc converters," *IEEE Trans. Aerosp. Electron. Syst.*, vol. 29, no. 3, pp. 1059–1063, Jul. 1993.

[65] A. Reatti and M. K. Kazimierczuk, "Small-signal model of PWM converters for discontinuous conduction mode and its application for boost converter," *IEEE Trans. Circuits Syst. I: Fundam. Theory Appl.*, vol. 50, no. 1, pp. 65–73, Jan. 2003.

[66] G. Zhu, S. Luo, C. Iannello, and I. Bataresh, "Modeling of conduction losses in PWM converters operating in discontinuous conduction mode," in *Proc. Int. Symp. Circuits Syst.*, May 2000, vol. 3, pp. 111–114.

[67] G. Nirgude, R. Tirumala, and N. Mohan, "A new, large-signal average model for single-switch DC-DC converters operating in both CCM and DCM," in *Proc. IEEE Power Electronics Specialists Conf.*, June 2001, vol. 3, pp. 1736–1741.

[68] I. Zafrany and S. Ben-Yaakov, "Generalized switched inductor model (GSIM): Accounting for conduction losses," *IEEE Trans. Aerosp. Electron. Syst.*, vol. 38, no. 2, pp. 681–687, Apr. 2002.

[69] A. Davoudi, J. Jatskevcih, and P. L. Chapman, "Averaged modeling of switched-inductor cells considering conduction losses in discontinuous mode," *Inst. Eng. Technol. Electric Power Appl.*, vol. 1, no. 3, pp. 402–406, May 2007.

[70] A. Davoudi, J. Jatskevich, P. L. Chapman, and A. Khaligh, "Averaged-switch modeling of fourth-order PWM dc-dc converters considering conduction losses in discontinuous mode," *IEEE Trans. Power Electron.*, vol. 22, no. 6, pp. 2410–2415, Nov. 2007.

[71] S. Cuk and R. D. Middlebrook, "A general unified approach to modeling switching DC-to-DC converters in discontinuous conduction mode," in *Proc. IEEE Power Electronics Specialists Conf.*, Jun. 1977, pp. 36–57.

[72] J. Sun, D. M. Mitchell, M. F. Greuel, P. T. Krein, and R. M. Bass, "Modeling of PWM converters in discontinuous conduction mode-A reexamination," in *Proc. IEEE Power Electronics Specialists Conf.*, May 1998, vol. 1, pp. 615–622.

[73] A. Davoudi and J. Jatskevich, "Parasitics realization in state-space average-value modeling of PWM dc-dc converters using an equal area method," *IEEE Trans. Circuits Syst. I, Reg. Papers*, vol. 54, no. 9, pp. 1960–1967, Sep. 2007.

[74] A. Davoudi and J. Jatskevich, "Realization of parasitics in state-space average-value modeling of PWM DC-DC converters," *IEEE Trans. Power Electron.*, vol. 21, no. 4, pp. 1142–1147, Jul. 2006.

[75] A. Davoudi, J. Jatskevich, and T. DeRybel, "Numerical state-space average-value modeling of PWM DC-DC converters operating in DCM and CCM," *IEEE Trans. Power Electron.*, vol. 21, no. 4, pp. 1002–1012, Jul. 2006.

[76] J. Jatskevich, S. D. Pekarek, and A. Davoudi, "Parametric average-value model of synchronous machine-rectifier systems," *IEEE Trans. Energy Convers.*, vol. 21, no. 1, pp. 9–18, Mar. 2006.

[77] A. Yazdani and R. Iravani, "A generalized state-space averaged model of the three-level NPC converter for systematic DC-voltage-balancer and current-controller design," *IEEE Trans. Power Del.*, vol. 20, no. 2, pt. 1, pp. 1105–1114, Apr. 2005.

[78] K. Corzine, K. Xiaomin, and J. R. Baker, "Dynamic average-value modeling of a four-level drive system," *IEEE Trans. Power Electron.*, vol. 18, no. 2, pp. 619–627, Mar. 2003.

[79] V. Caliskan, D. J. Perreault, T. M. Jahns, and J. G. Kassakian, "Analysis of three-phase rectifiers with constant-voltage loads," *IEEE Trans. Circuits Syst. I: Fundam. Theory Appl.*, vol. 50, no. 9, pp. 1220–1226, Sep. 2003.

[80] H. Zhu, "New multi-pulse diode rectifier average models for ac and dc power systems studies," Ph.D. dissertation, Virginia Polytechnic Inst. State Univ., Blacksburg, VA, 2005.

[81] H. Zhu, R. P. Burgos, F. Lacaux, A. Uan-Zo-li, D. K. Linder, F. Wang, and D. Boroyevich, "Average modeling of three-phase and nine-phase diode rectifiers with improved ac current and dc voltage dynamics," in *Proc. 31st Annu. Conf. IEEE Industrial Electron. Soc.*, Nov. 2005, pp. 1024–1029.

[82] P. Pejović and J. W. Kolar, "Exact analysis of three-phase rectifiers with constant voltage loads," *IEEE Trans. Circuits Syst. II: Expr. Briefs*, vol. 55, no. 8, pp. 743–747, Aug. 2008.

[83] S. D. Sudhoff and O. Wasynczuk, "Analysis and average-value modeling of line-commutated converter-synchronous machine systems," *IEEE Trans. Energy Convers.*, vol. 8, no. 1, pp. 92–99, Mar. 1993.

[84] S. D. Sudhoff, K. A. Corzine, H. J. Hegner, and D. E. Delisle, "Transient and dynamic average-value modeling of synchronous machine fed load-commutated converters," *IEEE Trans. Energy Convers.*, vol. 11, no. 3, pp. 508–514, Sep. 1996.

[85] J. T. Alt, S. D. Sudhoff, and B. E. Ladd, "Analysis and average-value modeling of an inductorless synchronous machine load commutated converter system," *IEEE Trans. Energy Convers.*, vol. 14, no. 1, pp. 37–43, Mar. 1999.

[86] I. Jadric, D. Borojevic, and M. Jadric, "A simplified model of a variable speed synchronous generator loaded with diode rectifier," in *Proc. 28th Annu. IEEE Power Electronics Specialists Conf.*, Jun. 1997, vol. 1, pp. 497–502.

[87] I. Jadric, D. Borojevic, and M. Jadric, "Modeling and control of a synchronous generator with an active DC load," *IEEE Trans. Power Electron.*, vol. 15, no. 2, pp. 303–311, Mar. 2000.

[88] J. Jatskevich, S. D. Pekarek, and A. Davoudi, "Fast procedure for constructing an accurate dynamic average-value model of synchronous machine-rectifier systems," *IEEE Trans. Energy Convers.*, vol. 21, no. 2, pp. 435–441, Jun. 2006.

[89] B. Zhang, "Modeling and analysis of source-commutated five-phase diode rectifier systems," Ph.D. dissertation, Univ. Missouri-Rolla, Rolla, MO, 2004.

[90] B. Zhang and S. D. Pekarek, "Analysis and average value model of a source-commutated 5-phase rectifier," in *Proc. 25th Annu. IEEE Power Electronics Specialists Conf.*, Jun. 2004, vol. 1, pp. 362–368.

[91] A. Baghramian and A. J. Forsyth, "Averaged-value models of twelve-pulse rectifiers for aerospace applications," in *Proc. 2nd Int. Conf. Power Electronics, Machines and Drives*, Mar./Apr. 2004, vol. 1, pp. 220–225.

[92] A. Cross, A. Baghramian, and A. Forsyth, "Approximate, average, dynamic models of uncontrolled rectifiers for aircraft applications," *Inst. Eng. Technol. Power Electron.*, vol. 2, no. 4, pp. 398–409, Jul. 2009.

[93] S. D. Sudhoff, "Analysis and average-value modeling of dual line-commutated converter- 6-phase synchronous machine systems," *IEEE Trans. Energy Convers.*, vol. 8, no. 3, pp. 411–417, Sep. 1993.

[94] J. Jatskevich, E. Walters, C. Lucas, and P. T. Lamm, "Average-value model of a high-frequency six-phase generation system," *SAE Trans. J. Aerosp.*, vol. 113, no. 1, pp. 1854–1861, Nov. 2004.

[95] J. Jatskevich and S. D. Pekarek, "Six-phase synchronous generator rectifier parametric average value modeling considering operational modes," *HAIT J. Sci. Eng. B*, vol. 2, no. 3–4, pp. 365–385, Dec. 2005.

[96] H. Zhu, R. P. Burgos, F. Lacaux, A. Uan-Zo-li, D. K. Linder, F. Wang, and D. Boroyevich, "Evaluation of average models for nine-phase diode rectifiers with improved ac and dc dynamics," in *Proc. 21st Annu. IEEE Applied Power Electronics Conf. Expo.*, Mar. 2006, pp. 1324–1330.

[97] S. Rosado, R. Burgos, F. Wang, and D. Boroyevich, "Large- and small-signal evaluation of average models for multi-pulse diode rectifiers," in *Proc. IEEE Workshop on Computer in Power Electronics*, Jul. 2006, pp. 89–94.

[98] H. W. Dommel, "Digital computer solution of electromagnetic transients in single- and multiphase networks," *IEEE Trans. Power App. Syst.*, vol. PAS-88, no. 4, pp. 388–399, Apr. 1969.

[99] H. W. Dommel, *EMTP Theory Book*. Vancouver, BC, Canada: MicroTran Power System Analysis Corp., 1992.

[100] J. Mahseredjian, V. Dinavahi, and J. A. Martinez, "Simulation tools for electromagnetic transients in power systems: Overview and challenges," *IEEE Trans. Power Del.*, vol. 24, no. 3, pp. 1657–1669, Jul. 2009.

[101] H. W. Dommel, "Nonlinear and time-varying elements in digital simulation of electromagnetic transients," *IEEE Trans. Power App. Syst.*, vol. PAS-90, no. 6, pp. 2561–2567, Nov./Dec. 1971.

[102] S. M. Chan and V. Brandwajn, "Partial matrix refactorization," *IEEE Trans. Power Syst.*, vol. PWRS-1, no. 1, pp. 193–200, Feb. 1986.

[103] K. Strunz, L. Linares, J. R. Marti, O. Huet, and X. Lombard, "Efficient and accurate representation of asynchronous network structure changing phenomena in digital real time simulators," *IEEE Trans. Power Syst.*, vol. 15, no. 2, pp. 586–592, May 2000.

[104] C. Dufour and J. Bélanger, "Discrete time compensation of switching events for accurate real-time simulation of power systems," in *Proc. 27th Annu. Conf. IEEE Industrial Electronics Soc.*, Nov./Dec. 2001, pp. 1533–1538.

[105] L. R. Linares and J. R. Marti, "A resynchronization algorithm for topological changes in real time fast transients simulation," presented at the 14th Power Systems Computation Conf., Sevilla, Spain, Jun. 2002.

[106] M. Zou, J. Mahseredjian, B. Delourme, and G. Joos, "On interpolation and reiniialization in the simulation of transients in power electronic systems," presented at the 14th Power Systems Computation Conf., Sevilla, Spain, Jun. 2002.

[107] K. Strunz, "Flexible numerical integration for efficient representation of switching in real time electromagnetic transients simulation," *IEEE Trans. Power Del.*, vol. 19, no. 3, pp. 1276–1283, Jul. 2004.

[108] M. O. Faruque, V. Dinavahi, and W. Xu, "Algorithms for the accounting of multiple switching events in the digital simulation of power electronic systems," *IEEE Trans. Power Del.*, vol. 20, no. 2, pt. 1, pp. 1157–1167, Apr. 2005.

[109] V. Dinavahi, M. R. Iravani, and R. Bonert, "Real-time digital simulation of power electronic apparatus interfaced with digital controllers," *IEEE Trans. Power Del.*, vol. 16, no. 4, pp. 775–781, Oct. 2001.

[110] J. R. Marti and J. Lin, "Suppression of numerical oscillations in the EMTP," *IEEE Trans. Power Syst.*, vol. 4, no. 2, pp. 739–747, May 1989.

[111] J. Lin and J. R. Marti, "Implementation of the CDA procedure in the EMTP," *IEEE Trans. Power Syst.*, vol. 5, no. 2, pp. 394–402, May 1990.

[112] M. O. Faruque, Y. Zhang, and V. Dinavahi, "Detailed modeling of CIGRÉ HVDC benchmark system using PSCAD/EMTDC and PSB/SIMULINK," *IEEE Trans. Power Del.*, vol. 21, no. 1, pp. 378–387, Jan. 2006.

[113] R. D. Middlebrook, "Input filter considerations in design and application of switching regulators," in *Proc. IEEE Industrial Applications Soc. Conf.*, Oct. 1976, pp. 91–107.

[114] M. B. Harris, A. W. Kelley, J. P. Rhode, and M. E. Baran, "Instrumentation for measurement of line impedance," in *Proc. 9th IEEE Applied Power Electronics Conf.*, Feb. 1994, vol. 2, pp. 887–893.

[115] S. D. Sudhoff, B. P. Loop, J. Byoun, and A. M. Cramer, "A new procedure for calculating immittance characteristics using detailed computer simulations," in *Proc. IEEE Power Electronics Specialists Conf.*, Jun. 2007, pp. 901–908.

[116] Z. Bing, K. J. Karimi, and J. Sun, "Input impedance modeling and analysis of line-commutated rectifiers," in *Proc. IEEE Power Electronics Specialists Conf.*, Jun. 2007, pp. 1981–1987.

[117] J. Sun and K. Karimi, "Small-signal input impedance modeling of line-frequency rectifiers," *IEEE Trans. Aerosp. Electron. Syst.*, vol. 44, no. 4, pp. 1489–1497, Oct. 2008.

[118] Z. Bing, K. J. Karimi, and J. Sun, "Input impedance modeling and analysis of line-commutated rectifiers," *IEEE Trans. Power Electron.*, vol. 24, no. 10, pp. 2338–2346, Oct. 2009.

[119] J. Huang, K. A. Corzine, and M. Belkhayat, "Small-signal impedance measurement of power-electronics-based ac power systems using line-to-line current injection," *IEEE Trans. Power Electron.*, vol. 24, no. 2, pp. 445–455, Feb. 2009.

[120] Y. A. Familiant, J. Huang, K. Corzine, and M. Belkhayat, "New techniques for measuring impedance characteristics of three-phase ac power systems," *IEEE Trans. Power Electron.*, vol. 24, no. 7, pp. 1802–1810, Jul. 2009.